Nonlinear Power Response in Heterodyne Photonic Radiometers for Microwave Remote Sensing

Charles J. Turner, *Member, IEEE*, Andrew I. Harris, *Member, IEEE*, Thomas E. Murphy, *Senior Member, IEEE*, and Mark Stephen

***Abstract*— Microwave photonic circuits are capable of processing large bandwidths of radiometric data (>100 GHz) in an unprecedented number of analog spectrometer channels (>100) at narrow spectral resolutions (<100 MHz) and a small device footprint. However, simultaneously processing this entire bandwidth requires a large dynamic range. In this work, a heterodyne photonic radiometer is assembled and tested with a microwave thermal noise source. We model and demonstrate the 1 dB output power compression point occurs at approximately half of the average input power for a thermal noise signal compared to a continuous wave signal. These results have a significant impact on future photonic radiometer design considerations.**

***Index Terms*— Remote sensing, microwave radiometry, microwave photonics.**

I. Introduction

MICROWAVE radiometers are used in atmospheric remote sensing and radio astronomy for measuring broadband radiation emissions. NASA and NOAA have an essential need across multiple missions for a broadband (>100 GHz) microwave radiometer that can simultaneously process the entire measured spectrum in hundreds of narrow spectral channels [1]. Additionally, instrument components are constrained to a limited size, weight, and power consumption (SWaP) for spaceborne platforms. Application-Specific Integrated Circuit (ASIC) digital spectrometers continue to improve in performance at low levels of power consumption, but currently at relatively limited instantaneous bandwidths and sampling speeds [2]. A microwave front-end consisting of traditional amplifiers, mixers, oscillators, and filters can channelize the measured spectrum into manageable chunks for digital sampling at each channel, but this increases SWaP due to the added components and additional digital spectrometers. Alternatively, Photonic Integrated Circuits (PICs) were identified as a candidate technology for the next generation of microwave radiometers [3], [4]. A hybrid PIC-ASIC solution can leverage both technologies to increase a radiometer's instantaneous bandwidth, process the entire measured spectrum, and minimize additional SWaP using different back-end channel bandwidths as needed. Integrated Micro-Ring Resonators (MRR) have been implemented as tunable band-pass filters with 3-dB-bandwidths below 200 MHz [5]. We propose implementing photonic down-conversion for digital sampling in the bands which require a finer spectral resolution than that attainable with photonic filters. Optical signal processing of radiometric microwave signals with bulk components has been applied to millimeter-wavelength signal detection [6], W-band imagery [7], and improving the noise-equivalent temperature (NET) in narrow-band radiometers [8] and radiometric resolutions in interferometers [9]. However, these efforts did not leverage the full bandwidth and integrated platform possible in more recent PIC advancements. Now, integrated Electro-Optic Modulators (EOM) with CMOS-compatible voltages are capable of modulation bandwidths above 100 GHz [10]. Previous work did not extensively investigate the dynamic range of microwave photonic radiometers with photonic down-conversion. Here, we report on impact of signal type to radiometer linearity.

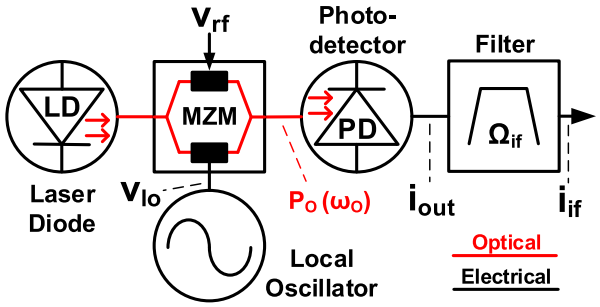

Fig. 1. Block diagram for the single-channel microwave photonic radiometer.

This work investigates the dynamic range of a single-channel photonic radiometer. Dynamic range refers to the range of measurable microwave power between the instrument's noise floor and an upper limit set by the required linearity of its power response. We demonstrate a significant and measurable impact to its dynamic range while taking radiometric measurements. In practice, a radiometric measurement requires a highly-linear calibration measurement of two temperature references. This helps distinguish between a change in measured noise power from the target and detection of local temperature, power, or gain

Manuscript received 7 February 2023; revised 12 April 2023; accepted 27 April 2023. Date of publication 5 May 2023; date of current version 22 May 2023. *(Corresponding author: Charles J. Turner.)*

Charles J. Turner, Andrew I. Harris, and Thomas E. Murphy are with the Department of Electrical and Computer Engineering, University of Maryland, College Park, MD 20742 USA (e-mail: cjturner@umd.edu; aharris1@umd.edu; tem@umd.edu).

Mark Stephen is with the NASA Goddard Space Flight Center, Greenbelt, MD 20771 USA (e-mail: mark.a.stephen@nasa.gov).

Color versions of one or more figures in this letter are available at https://doi.org/10.1109/LPT.2023.3273412.

Digital Object Identifier 10.1109/LPT.2023.3273412

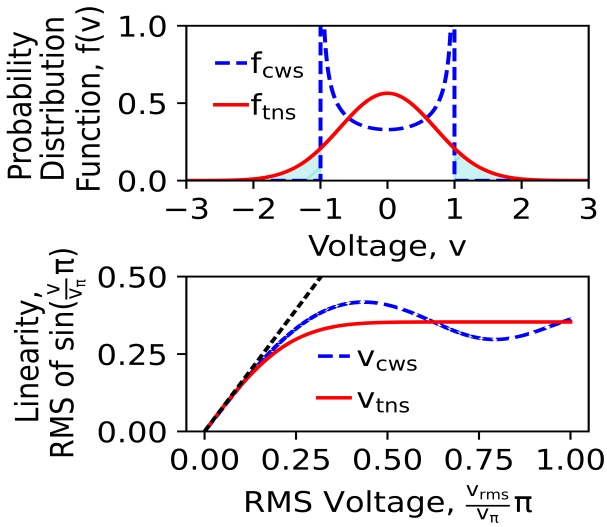

Fig. 2. (Top) probability distribution function and (bottom) difference in linearity of Eq. 4 for CWS and TNS.

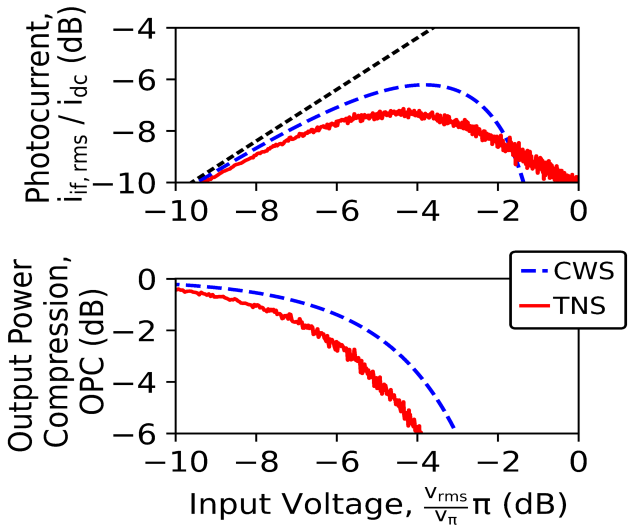

Fig. 3. (Top) Simulated IF photocurrent and (bottom) output power compression at photodetector output.

fluctuations [11]. An accurate nonlinear model and instrument characterization can help reduce measurement uncertainty and improve the dynamic range. This test radiometer exhibits a larger nonlinear response to a thermal noise signal (TNS) than a Continuous Wave Signal (CWS) more commonly referenced in literature [12]. Our measurement results agree with our new stochastic nonlinear power response model and simulation. These results support investigations into the feasibility of developing a microwave photonic radiometer with a noise figure and dynamic range that meet specific mission requirements.

II. Theory

A Photonic Down-Converter (PDC) reduces the measured signal's carrier radio frequency (Ω_{rf}) to a smaller intermediate frequency (Ω_{if}) through mixing with a local oscillator frequency (Ω_{lo}) [12], [13], [14], [15], [16]. With down-conversion and filtering, the output channel bandwidth is small enough for digital sampling. The derivations presented here are applicable to multiple PDC architectures. A non-modulated CWS consists of a cosine function with an amplitude voltage of v:

$$v_{cws}(t) = v\cos(\Omega_{rf}t + \Delta\theta) \tag{1}$$

where Ω_{rf} represents its frequency and $\Delta\theta$ is used to account for a potential phase difference between itself and CWS LO signal. The probability of measuring some voltage at any instant is well known for this signal and described by its probability density function (PDF):

$$f_{cws}(v) = \frac{1}{\pi}(2v_{rms}^2 - v^2)^{-\frac{1}{2}} \tag{2}$$

where v is the measured voltage and $v_{rms} = \sqrt{\langle v^2\rangle}$ is the root-mean-square (RMS) average voltage measured over a defined number of samples. In constrast, a TNS represents thermal noise power from blackbody radiation emissions. Its PDF follows a Gaussian or normal distribution:

$$f_{tns}(v) = \frac{1}{\sqrt{2\pi}\,v_{rms}}\exp\left(-\frac{1}{2}\frac{v^2}{v_{rms}^2}\right) \tag{3}$$

The differences in these PDF's are illustrated in Fig. 2 where f_{cws} and f_{tns} have both been constrained to share the same time-average value ($v_{rms} = 1/\sqrt{2}$). The CWS is constrained within its peak voltage of $v = 1$ and the TNS has a broader voltage distribution which exceeds this peak voltage. The probability of measuring a higher voltage with a TNS compared to a CWS is approximately 15.37%. This probability area is highlighted in cyan. When applied as an input to a nonlinear system, the average output measurement will change as a result of these different voltage distributions.

A PDC's output photocurrent is presented here [16]:

$$i_{out}(t) = \frac{\alpha}{2}i_{dc}J_1\left(\frac{\pi}{v_\pi}v_{lo}\right)\sin\left(\frac{\pi}{v_\pi}v_{rf}(t)\right) \tag{4}$$

where v_π represents the sensitivity of the Dual-Drive Mach Zehnder Modulator (DD-MZM), and α is a scaling factor that accounts for insertion losses due to differences in PDC architectures. The limiting component to a PDC's linearity is the EOM, so the DC photocurrent $i_{dc} = RP_0$ is taken as a constant. i_{dc} is a product of the optical power (P_0) applied to a photodetector with a responsivity (R). The key non-linear term in Eq. 4 is the sine function and Fig. 2 highlights the change in response to $i_{out}(t)$ given $v_{rf} = v_{cws}$ or $v_{rf} = v_{tns}$.

The photocurrent measured at the output of the photodetector is a summation of multiple frequency-dependent terms:

$$i_{out}(t) = i_{dc} + i'_{rf}(\Omega_{rf}t) + i'_{lo}(\Omega_{lo}t) + i_{if}(\Omega_{if}t) + \ldots \tag{5}$$

where $\Omega_{if} = \Omega_{rf} - \Omega_{lo}$, $i'_{rf}(t)$ and $i'_{lo}(t)$ are leakage currents from the RF and LO signal measured at the photodetector. There are additional intermodulation products (sum-frequency, harmonics, etc) not shown here and are assumed to be suppressed through filtering. The output photocurrent (i_{out}) is filtered with an electronic band-pass filter (BPF) to isolate the desired IF term. The IF photocurrent can be determined by a

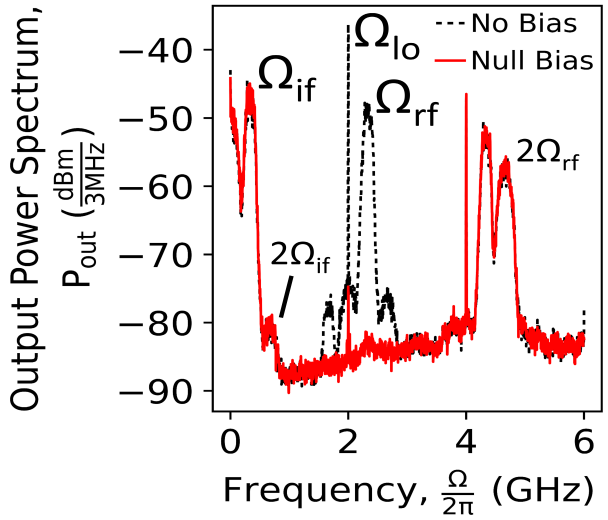

Fig. 4. Electrical output power spectrum measured over 3 MHz resolution bins at PDC output.

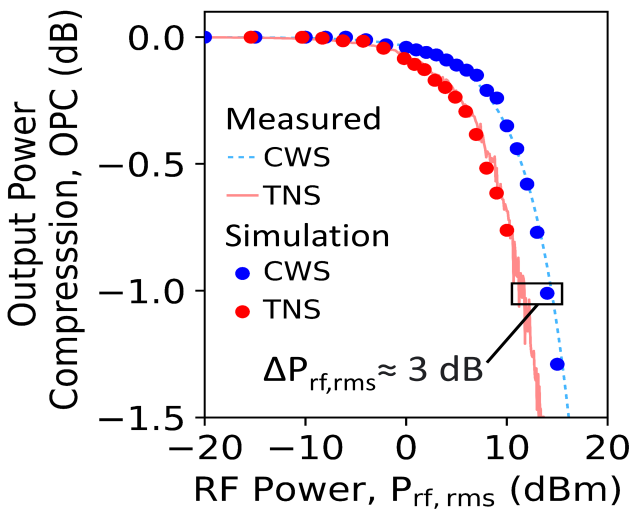

Fig. 5. Output power compression (OPC) simulation and measurements for the IF component of the spectrum for an incident TNS and CWS.

numerical simulation using Fourier analysis. The Fourier analysis of random sequences has been previously discussed [17] and successfully applied in white noise models [18]. The TNS is described with the following equation:

$$v_{tns}(t) = \sum_{k=1}^{N/2} v_k \cos(\Omega_{rf,k} t + \phi_k) \tag{6}$$

With this method, the TNS is modeled as a superposition of some number of cosine terms (N), equally-spaced in frequency ($\Omega_{rf,k}$), each with its own peak voltage (v_k) and phase (ϕ_k). ϕ_k is independently and randomly chosen over a uniform distribution from $[0, 2\pi)$ for one period. This summation has a few noteworthy advantages. Each v_k term can be identically distributed to correspond to white noise, or each given a mean value to more accurately model the frequency-dependent losses of the microwave components. Also, the number of samples and cosine terms can be conveniently chosen for clean conversion between the time and frequency domains in simulation using a Fast Fourier Transform (FFT).

Fig. 3 presents simulation results for the IF photocurrent. i_{if} is found through a FFT of i_{out} where Eq. 1 and Eq. 6 are applied to Eq. 4 for a CWS and TNS signal respectively. For each value of $v_{rf,rms}$, the TNS is generated in the frequency domain with N=4096 frequency terms. Each phase term is selected for one full period, which is determined by the lowest-frequency term. $\alpha = 1$ and v_{lo} is selected to achieve a maximum value for $J_1(v_{lo})$. Output Power Compression (OPC) is defined as the deviation in PDC output power from a linear response to input power. It may also be referred to as gain compression since the gain is reduced from its constant small-signal-approximation value. It can be expressed as:

$$OPC = \frac{P_{if,rms}}{P_{if,rms,ss}} = \frac{i^2_{if,rms}}{i^2_{if,rms,ss}} = \frac{G_{pdc}}{G_{pdc,ss}} \tag{7}$$

where $P_{if,rms,ss}$ and $G_{if,ss}$ are the small-signal, root-mean-square IF power and conversion gain for the PDC. In the same simulation, the OPC is found using this equation and plotted in Fig. 3. In the linear and nonlinear regions at lower voltage levels, i_{out} and OPC are in close agreement. However, the response starts to diverge prior to the OP1, the point at which the output power compresses from linearity by 1 dB.

III. Experimental Results

The single-channel microwave photonic radiometer was assembled with components as depicted in Fig. 1. It consisted of a 1550 nm DFB Laser Diode (LD), A $v_\pi = 5.5$ V Dual-Drive Mach Zehnder Modulator (DD-MZM), Photodetector (PD), and IF Band-Pass Filter (BPF). An adjustable noise source provided the TNS to the radiometer input. We assembled the noise source with a cascade of available amplifiers, attenuators, and filters. This noise source can produce a maximum total power of nearly 10 dBm with a center frequency of 2.3 GHz and a 3-dB-bandwidth of 140 MHz.

Fig. 4 presents the electrical output power spectrum of the PDC measured with a spectrum analyzer. These results demonstrate the unique behavior of this photonic radiometer using TNS instead of a modulated CWS, and compared to a traditional microwave radiometer with mixers. The noise source provided its maximum 10 dBm of RF power, the LD provided 16 dBm of optical power, and a signal generator provided 10 dBm of LO power. The linearity of the photodetector and spectrum analyzer detector were verified by sweeping the optical power and monitoring the measurement for a nonlinear response. The spectrum analyzer measured the power in 3 MHz bins. The IF BPF was removed for this test in order to measure the various intermodulation products. The noise source's relatively narrow bandwidth minimized overlap of the various intermodulation products measured at the radiometer's output. There is a second-order distortion visible near DC, likely caused by rectification of the RF signal. The LO frequency was selected at 2 GHz to isolate the IF term from this distortion. The resulting IF frequency is 0.3 GHz. Leakage from the RF and LO signals are visible and identified, as well as a few other intermodulation terms. Many of these

output terms can be suppressed by applying a DC bias voltage to one of the DD-MZM inputs, something not possible with microwave mixers. The DD-MZM can be biased to "null" to suppress odd-order terms, including the RF and LO leakage terms [19]. This simplifies filtering at the output except for the baseband distortion. Biasing the DD-MZM to "quadrature" will suppress even-order terms such as this distortion, but also the IF term. In a future effort, we will seek to suppress the baseband noise with an alternative PDC architecture.

We tested the PDC's nonlinear power response using both a CWS and TNS and report the results in Fig. 5. The measurements showed close agreement with simulation for both an applied CWS and TNS. We found the applied RF power for a TNS is approximately 3 dB lower than a CWS at the OP1 point of the PDC. This is a significant difference and should be taken as a design consideration for a future, complete photonic radiometer instrument. We connected a BPF to the output of a signal generator to provide a clean CWS to the DD-MZM input. The TNS output power was adjusted automatically by an Arduino-controlled digital-step attenuator. This allowed us to repeat the measurements in multiple iterations and verify there were no significant gain fluctuations over longer time scales (> 1 s). We measured the output power for both of these devices and likewise monitored for any nonlinear contributions to the final measurement. The input power was swept to the highest possible power level for our noise source and signal generator, which allowed us to measure close to the OP1. We applied each signal to the input of the radiometer and measured the output with a BPF connected to isolate the IF photocurrent. The gain is taken as the ratio between the measured output and input powers. Using Eq. 7, we found the resulting OPC by normalizing the measured gain to its small-signal gain.

IV. Conclusion

We have characterized and measured the nonlinear power response of a single-channel microwave photonic radiometer for radiometric measurements. We found the output power compresses by 1 dB (OP1) at nearly half the average RF input power for a thermal noise signal than for a continuous-wave signal. These results are important for ongoing photonic radiometer design efforts due to the large bandwidths and noise contributions associated with photonics. At higher optical powers, the noise figure of photonic down-converters are limited by the laser's relative intensity noise (RIN) [20]. A 20 dBm laser with an average RIN of -160 dBc/Hz will emit -30 dBm of noise power over 100 GHz bandwidth. -20 dBm of signal power applied to the photodetector would maintain a typical signal-to-noise ratio of 10 dB for digital sampling. The required RF signal power would be higher to overcome additional noise sources and electrical-to-optical conversion losses, but -20 dBm is already near the non-linear region of our test radiometer. In this scenario, our model would improve error correction for a radiometer calibration.

References

[1] C. D. Kummerow et al., "Hyperspectral microwave sensors—Advantages and limitations," *IEEE J. Sel. Topics Appl. Earth Observ. Remote Sens.*, vol. 15, pp. 764–775, 2022.

[2] F. Hsiao, A. Tang, Y. Kim, B. Drouin, G. Chattopadhyay, and M.-C.-F. Chang, "A 2.2 GS/s 188 mW spectrometer processor in 65 nm CMOS for supporting low-power THz planetary instruments," in *Proc. IEEE Custom Integr. Circuits Conf. (CICC)*, Sep. 2015, pp. 1–3.

[3] J. Teixeira et al., "Toward a global planetary boundary layer observing system: The NASA PBL incubation study team report," PBL Incubation Study Team, NASA, Washington, DC, USA, Tech. Rep. 134, 2021. [Online]. Available: https://science.nasa.gov/earth-science/decadal-pbl

[4] A. Gambacorta et al., "The hyperspectral microwave photonic instrument (HYMPI)—Advancing our understanding of the earth's planetary boundary layer from space," in *Proc. IEEE Int. Geosci. Remote Sens. Symp. (IGARSS)*, Jul. 2022, pp. 4468–4471.

[5] T. Pett, J. H. Lee, Y. Ehrlichman, H. Gevorgyan, A. Khilo, and M. Popovic, "Photonics-based microwave radiometer for hyperspectral Earth remote sensing," in *Proc. Int. Topical Meeting Microw. Photon. (MWP)*, 2018, pp. 1–4.

[6] C. A. Schuetz, J. Murakowski, G. J. Schneider, and D. W. Prather, "Radiometric millimeter-wave detection via optical upconversion and carrier suppression," *IEEE Trans. Microw. Theory Techn.*, vol. 53, no. 5, pp. 1732–1738, May 2005.

[7] T. Dillon et al., "Compact passive millimeter wave imager for degraded visual and GPS-denied navigation," in *Proc. IEEE Res. Appl. Photon. Defense Conf. (RAPID)*, Aug. 2019, pp. 19–22.

[8] G. S. Botello et al., "Sensitivity limits of millimeter-wave photonic radiometers based on efficient electro-optic upconverters," *Optica*, vol. 5, no. 10, pp. 1210–1219, 2018.

[9] E. Nova, J. Romeu, S. Capdevila, F. Torres, and L. Jofre, "Optical signal processor for millimeter-wave interferometric radiometry," *IEEE Trans. Geosci. Remote Sens.*, vol. 52, no. 5, pp. 2357–2368, May 2014.

[10] C. Wang et al., "Integrated lithium niobate electro-optic modulators operating at CMOS-compatible voltages," *Nature*, vol. 562, pp. 101–104, Sep. 2018, doi: 10.1038/s41586-018-0551-y.

[11] F. Ulaby and D. Long, *Microwave Radar and Radiometric Remote Sensing*. Ann Arbor, MI, USA: University of Michigan Press, 2014.

[12] A. C. Lindsay, G. A. Knight, and S. T. Winnall, "Photonic mixers for wide bandwidth RF receiver applications," *IEEE Trans. Microw. Theory Techn.*, vol. 43, no. 9, pp. 2311–2317, Sep. 1995.

[13] G. K. Gopalakrishnan, R. P. Moeller, M. M. Howerton, W. K. Burns, K. J. Williams, and R. D. Esman, "A low-loss downconverting analog fiber-optic link," *IEEE Trans. Microw. Theory Techn.*, vol. 43, no. 9, pp. 2318–2323, Sep. 1995. [Online]. Available: http://ieeexplore.ieee.org/document/414584/

[14] V. R. Pagán, B. M. Haas, and T. E. Murphy, "Linearized electrooptic microwave downconversion using phase modulation and optical filtering," *Opt. Exp.*, vol. 19, no. 2, p. 883, Jan. 2011. [Online]. Available: http://ieeexplore.ieee.org/document/5645647/ and https://opg.optica.org/oe/abstract.cfm?uri=oe-19-2-883

[15] Y. Wang et al., "All-optical microwave photonic downconverter with tunable phase shift," *IEEE Photon. J.*, vol. 9, no. 6, pp. 1–8, Dec. 2017.

[16] S. T. Lipkowitz, T. U. Horton, and T. E. Murphy, "Wideband microwave electro-optic image rejection mixer," *Opt. Lett.*, vol. 44, no. 19, p. 4710, 2019.

[17] C. Lanczos and B. Gellai, "Fourier analysis of random sequences," *Comput. Math. Appl.*, vol. 1, nos. 3–4, pp. 269–276, 1975. [Online]. Available: https://www.sciencedirect.com/science/article/pii/0898122175900255, doi: 10.1016/0898-1221(75)90025-5.

[18] J. A. Grauer, "Random noise generation using Fourier series," *J. Aircr.*, vol. 55, no. 4, pp. 1753–1759, 2018.

[19] V. J. Urick, J. D. Mckinney, and K. J. Williams, *Fundamentals of Microwave Photonics*. Hoboken, NJ, USA: Wiley, Feb. 2015, doi: 10.1002/9781119029816.

[20] F. Bucholtz, M. J. Mondich, J. M. Singley, J. D. Mckinney, and K. J. Williams, "The noise figure of analog RF photonic receivers: Simple links, WDM links, and WDM receive-mode beamformers," Naval Res. Lab., Washington, DC, USA, Tech. Rep. NRL/MR/5651–20-10,094, 2020. [Online]. Available: https://apps.dtic.mil/sti/pdfs/AD1109440.pdf